CTFF3 TECHNICAL NOTE

INFN - LNF, Accelerator Division

Frascati, April 4, 2001

Note: **CTFF3-002**

COMBINER RING LATTICE

C. Biscari

1. Introduction

The 3rd CLIC test facility, CTF3, is foreseen to check the feasibility of pulse compression in the driving beam structure [1]. The facility will be installed at CERN, in the existing LIL and EPA buildings, which have become available after LEP shutdown. It will use the existing 3 GHz klystrons and modulators for the production of the beam. The pulse is 4.5 μs long, and is a sequence of "odd" and "even" bunch trains, whose duration, 140 ns, is determined by the gun. The separation between adjacent bunches is twice the rf wavelength, 20 cm.

The first compression is done in the delay loop with a length equal to the bunch train, 42 m, where the odd and even buckets are recombined, resulting in a bunch separation of 10 cm [2].

In the second compression phase the bunches are injected in the combiner ring, 84 m plus λ/5 long, twice the delay loop. Each group of 5 bunch trains does n+1/2 turns inside the ring, with n = 0,1,2,3,4, after what they are extracted by a kicker, with a flat top of at least 140ns. The bunch separation at this stage is 2cm.

The main requirements on the ring are the necessity of preserving the beam emittance and the longitudinal correlation during the compression and to maintain the same characteristics between bunches which make different number of turns.

A general design of the Combiner Ring has been already described [3]. A more detailed solution is described in this note, where the updated characteristics of the EPA magnets have been included in the optical model after the check on the compatibility of their actual dimensions in the layout [4].

2. Combiner Ring Lattice and Magnetic Layout

The ring consists of four isochronous arcs, two short sections housing wiggler magnets for path length tuning and two symmetric opposite long sections for injection and extraction. Quadrupole doublets around the arcs are used for matching. The layout of the ring[4] is shown in Fig. 1 and the main parameters are listed in Table I. The emittance and the energy spread refer to the injected beam characteristics which have been used for the design.

Table II refers to the magnets (dipoles, quadrupoles and sextupoles) used in the design, specifying their number, maximum gradients and reference to the list of EPA magnets [5]. The condition of reaching energies of 350 MeV prevents the use of the smaller type of EPA quadrupoles (type 4.8.1 [5]), whose maximum integrated gradient is only 0.5 T. The twelve available quadrupoles of type 4.8.2 are used two per arc and two in each wiggler section. All the other quadrupoles correspond to the type 5.3. The compatibility with the buildings and general layout has been checked. The compatibility with correctors and diagnostics must still be controlled; due to the large dimensions of this last type of quadrupoles it could be necessary to change some of them with smaller quadrupoles, of the same type of the DAFNE Accumulator [6]. The two family numbers listed in the table correspond to two conditions. The minimum number corresponds to the exact 4-fold symmetry, which needs only 9 families. The preferred configuration corresponds to the possibility of differentiating the injection from the extraction section (4 additional families added) and the two wiggler sections (2 more families), still maintaining all the arcs equal. The sextupoles are of the same type of the DAFNE Accumulator [7].

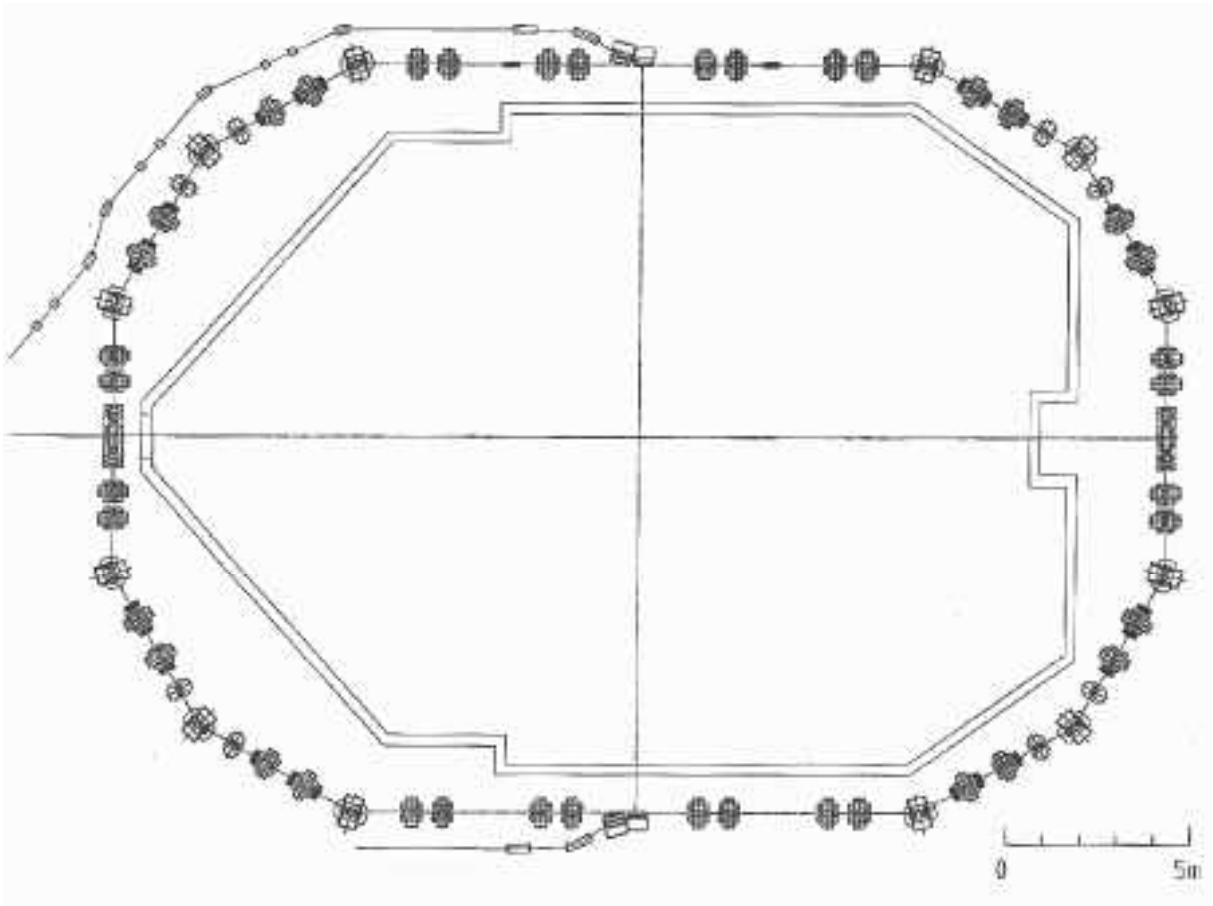

Figure 1: Combiner ring layout.

Table I – CR main parameters

Energy (MeV)	180/350
Bρ (T m)	0.60/1.17
Circumference (m)	84
No. Cells	4
Max. beta (m) (H/V)	11.1/11.1
Max. Dispersion (m)	.72
Betatron Tune (H/V)	7.23/4.14
Chromaticity (H/V)	-12.0/ -8.8
Momentum compaction	$<10^{-4}$
Horizontal emittance (mm mrad)	1/0.5
Vertical emittance (mm mrad)	1/0.5
Energy spread (%)	±1
Energy acceptance (%)	±2.5

Table II – CR magnets

A) N. of Dipoles (type 4.7)	12
Dipole Field (T)	0.55/1.07
Dipole Bending Radius [m]	1.09
Pole width [mm]	230
Gap height [mm]	45
B) N. of Quadrupoles	48
N. of Quadrupoles (type 4.8.2)	12
Magnetic length [m]	0.38
Maximum K_1 [m^{-2}]	2.24
Maximum Integrated gradient [T/m]	0.51/0.99
Quadrupole families (minimum/preferred)	2/3
Pole width [mm]	140
Available aperture [mm]	200
N. of Quadrupoles (type 5.3)	36
Magnetic length [m]	0.38
Maximum K_1 [m^{-2}]	3.54
Maximum Integrated Gradient [T]	0.81/1.57
Quadrupole families (minimum/preferred)	7/12
Pole width [mm]	134
Available aperture [mm]	184
C) N. of sextupoles	24
Magnetic length [m]	0.10
Maximum K_2 [m^{-3}]	100
Max Integrated Gradient [T/m]	6/11.7
Sextupole families	3
Available aperture [mm]	108
D) N. of Path Length Tuning Wigglers	2
Pole width [mm]	150
Gap height [mm]	40
Total length [m]	1.6
Number of half/full poles	2/1
Nominal Bending Radius [m]	3.3
Nominal field [T]	0.18/0.36

2.1 Isochronous Arc

The arcs are triple bend achromats, with negative dispersion in the central dipole, which makes the term of the first order transport matrix, relating path length with energy, vanish.

$$R_{56} = \int \frac{D_x}{\rho} \, ds = 0$$

where D_x is the dispersion and ρ the bending radius.

Three quadrupoles in each half arc allow tunability of betatron functions and tunes. Tuning two of the arc quadrupoles by few percent is the simple knob, which varies the momentum compaction α_c around zero. The value of the dispersion in the midpoint of the central dipole in each arc (D_o) is related to the value of the momentum compaction α_c by:

$$D_o \text{ (m)} = 40.218 \, \alpha_c - 0.10278$$

Figure 2 shows the amount of variation of α_c obtained by changing the gradient of the outer focusing quadrupoles by ±7%, and the defocusing ones by less than 2%. In this range the rest of ring can be easily matched to control tunes and optical functions.

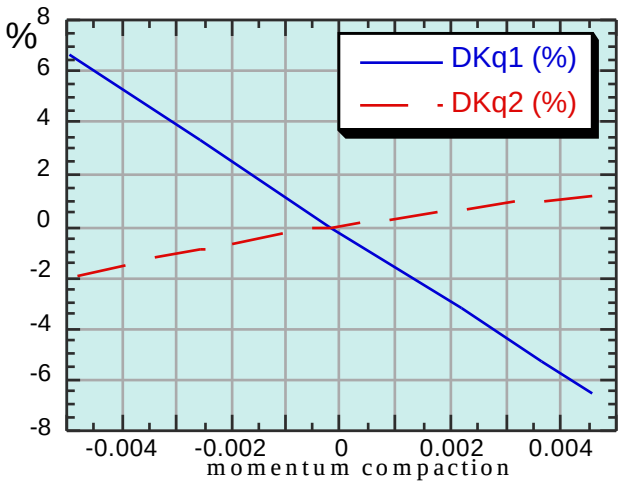

Figure 2: Relative change in the gradients of two arc quadrupole families to tune α_c.

2.2 Injection and Extraction

Equal structures are designed for the injection and extraction regions, which have similar requirements, thus doubling the ring periodicity. Injection and extraction septa are placed symmetrically (see Fig. 1) in the middle of a straight section 3.08 m long. The RF deflectors and the extraction kicker are placed in a free zone, 2.32 m long. The π phase advance in between the two injection deflectors is created by four quadrupoles arranged symmetrically around the septum. In the extraction region this assures the necessary $\pi/2$ phase advance between the extraction kicker and the septum. The space corresponding to the second kicker can be used to house an rf cavity in the hypothesis of storing the beam for diagnostic purposes.

A critical issue is the value of the horizontal betatron function, β_{xk}, at the fast rf injection kickers, affecting the amount of beam loading of the successive turns [3].

Values of $\beta_{xk} \sim 1.$ m and $\alpha_{xk} \sim 0$ correspond to minimum beam loading. The design allows the necessary tunability. The optical functions from the middle of the arc to the injection section are shown in Fig. 3.

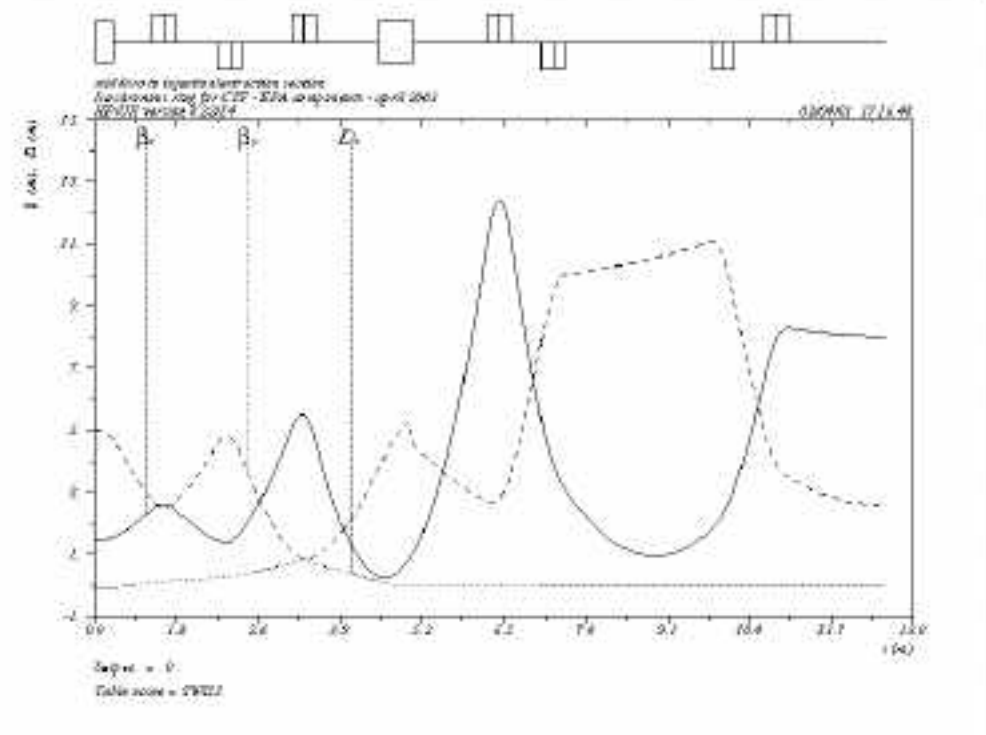

Figure 3: Optical functions from mid arc to injection/extraction.

2.3 Path-length tuning section

The tuning of the relative phase of injected and circulating bunches and the compensation of orbit variations is needed twice in the ring, to adjust independently each bunch train. The path-length tuning devices are variable field, single period wiggler magnets, housed in the short straight sections. With respect to a magnetic chicane the wiggler offers the advantages to be more compact, with a larger tuning range, and a lower contribution to the R_{56} term. It has two half end poles and a central one, independently powered, with bending angles –7°, 14°, -7° and a total length 1.6 m. The dispersion function introduced by the wiggler is selfmatched and the contribution to the momentum compaction, $-5\ 10^{-3}$ per wiggler, is compensated inside the arcs.

Changing the field by ±6% the path length variation is ± 0.5mm, which is the original requirement [1]. The tunability of the wiggler is an order of magnitude higher: the path length variation from the wigglers field off to a field value 50% higher than the nominal one corresponds to –4/+5 mm per wiggler. Figure 4 shows the path length variation as a function of the wiggler field and the corresponding value of the maximum horizontal displacement of the orbit from the ring axis. It is clear that if the whole range of the wiggler tunability is to be used, the horizontal aperture requirements increase. The change in the betatron tunes and momentum compaction of the whole ring for a single wiggler field variation are shown in Fig. 5, while Fig. 6 shows the corresponding change in the wiggler section quadrupole families. The isochronicity condition can be in any case recovered by tuning the arc R_{56} (see Fig. 2).

The optical functions from the arc center to the wiggler center are shown in Fig. 7 for the nominal case.

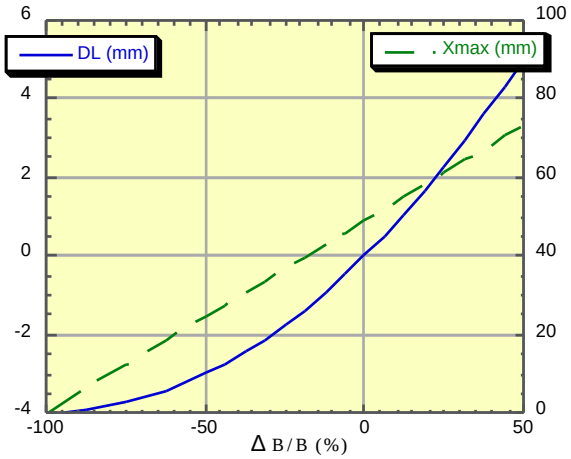

Figure 4: Path length variation (full line) as a function of wiggler field and maximum transverse displacement of the trajectory (dashed line).

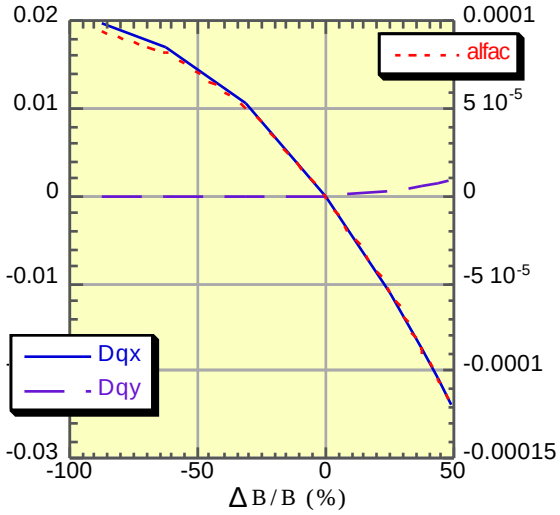

Figure 5– Momentum compaction and change in betatron tunes as a function of wiggler field.

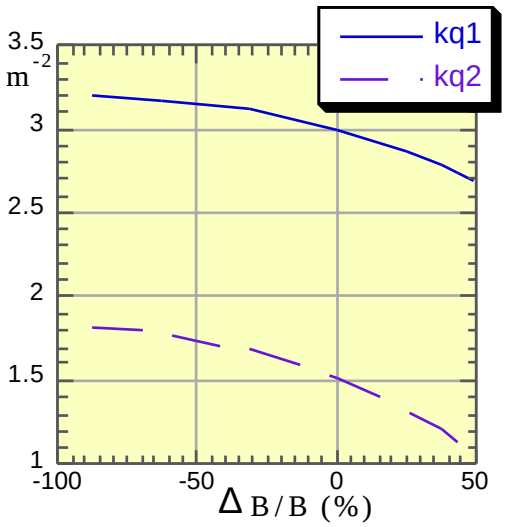

Figure 6 - Strength of the wiggler section quadrupoles which match transverse betatron waists at the wiggler center as a function of wiggler field.

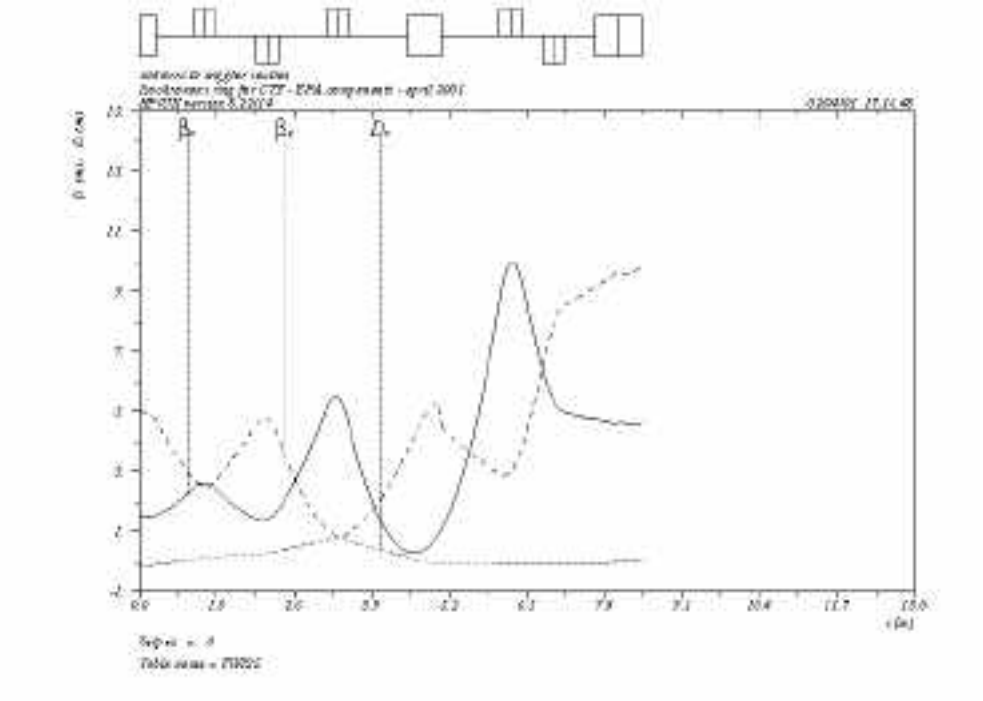

Figure 7: Optical functions from mid arc to wiggler center.

3. Beam size and apertures

The beam size along the ring has been computed with the parameters corresponding to the lowest energy ($\varepsilon_x = \varepsilon_y = 1$ mm mrad), which are the most demanding.

Figure 8 shows the behavior in one quarter of the ring of the horizontal beam envelope $\sigma_x = \sqrt{\beta_x \varepsilon_x}$ (full line), the horizontal beam envelope $\sigma_{xp} = D_x \Delta p / p$ due to 1% energy spread (dots) and the vertical envelope $\sigma_y = \sqrt{\beta_y \varepsilon_y}$ (dashed lines).

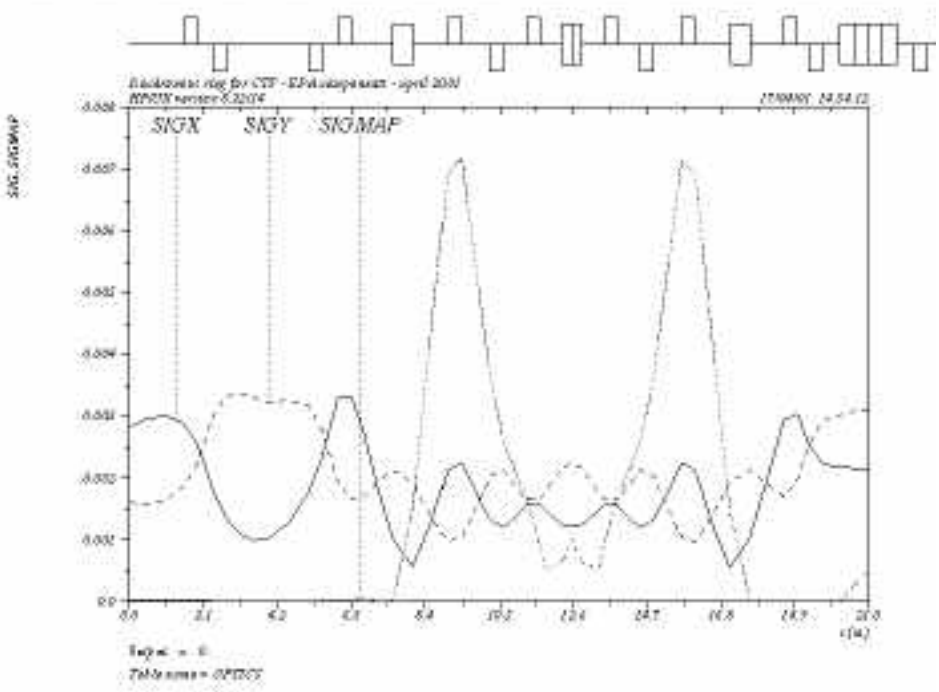

Figure 8: Beam size (one sigma) in a quarter of the ring.

The proposed vacuum chamber aperture [8] is (90 x 36) mm^2 (H x V) all around the ring, except in the injection/extraction sections where it has a round cross section (Ø = 40 mm). In the wiggler section the horizontal aperture is still being defined, since it depends on how much the wiggler tunability can be exploited. Figures 9 and 10 show that the aperture acceptance of the ring is ± $6\sigma_{x,y}$ and ± 4% of energy spread.

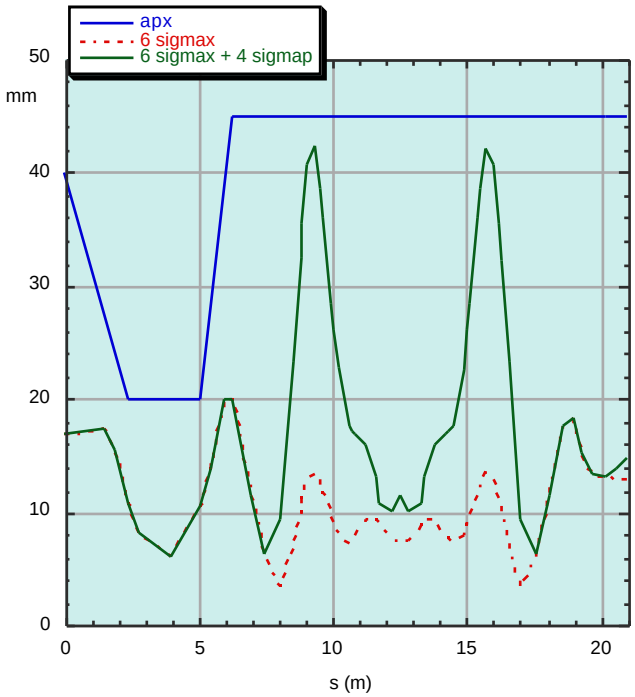

Figure 9: Horizontal beam size (six sigmas), momentum spread (4%) and horizontal aperture in a quarter of the ring.

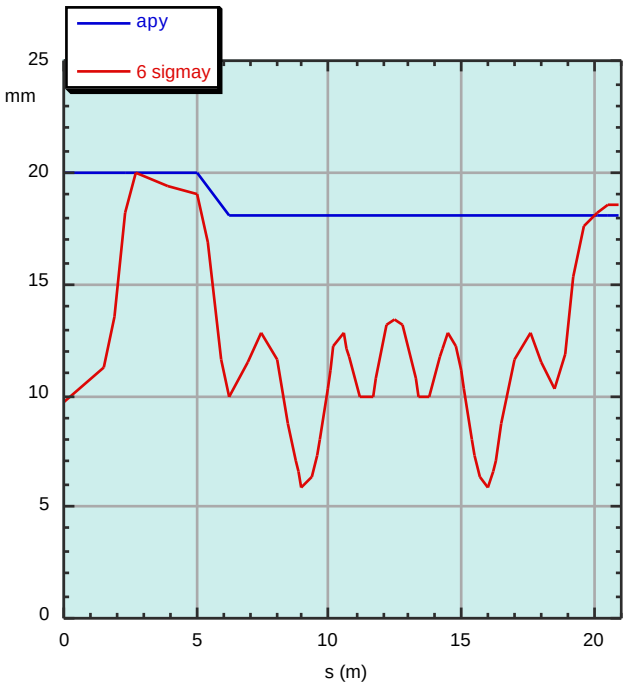

Figure 10: Beam size (six sigma) and vertical aperture in a quarter of the ring.

4 Isochronicity

The path length variation with energy is given up to the second order by:

$$c\Delta t = R_{56}\frac{\Delta p}{p} + T_{566}\left(\frac{\Delta p}{p}\right)^2 + \ldots$$

where T_{566} is the element of the second-order transfer matrix.

Isochronicity to the first order is assured by the zero integral of the dispersion function in each arc of the ring. Particles with energy deviations ±2.5% and with zero transverse initial invariant change their path length by up to 2.5 cm, with a clear second order dependence (see Fig. 10); even going to α_c values of few 10^{-2}, the second order term is still dominant.

The cancellation of the second order term is performed by sextupoles. A focusing sextupole in each arc can do the job but this solution, increasing the negative vertical chromaticity leads to isochronicity loss in the presence of vertical oscillations. The best solution is a compromise between the T_{566} cancellation and the chromaticity correction. A possible solution, which can still be improved, is the use of three sextupoles in each half arc, which give T_{566} = 0.00 and chromaticity of –0.9, -9.8 in the horizontal and vertical plane respectively.

Tracking with the MAD code has been performed for particles with energy deviations up to ±2.5%. Figure 11 shows the longitudinal and the horizontal phase planes of particles tracked for five turns in the case of no sextupoles in the ring. Figure 11a corresponds to particles with zero transverse invariant, Fig. 11b to particles with horizontal invariant $W_x = 1\ \sigma_x$, Fig. 11c to $W_x = 3\ \sigma_x$ and Fig. 11d to $W_x = 6\ \sigma_x$. The scales in the longitudinal phase plots are the same in the four cases, the scales in the first two cases of the horizontal phase plane plots are equal and multiplied by 3 and by 6 in the following two cases. The corresponding vertical plane is always zero in all cases. We observe that the neat 2nd order dependence of path length with energy deviation for particles with no transverse invariant is distorted and increased as the particle oscillates in the horizontal plane.

Figure 12 corresponds to the same particles in the case with sextupoles on. The 2nd order isochronicity is corrected. The distortion in the longitudinal phase space is still present, but smaller than before. To be noticed that the horizontal scale of the longitudinal phase plane plots is lowered by a factor ~2 with respect to Fig. 9, while the other scales are unchanged.

Figure 13 corresponds to particles with vertical invariants $(0, \sigma_y, 3\sigma_y, 6\sigma_y)$. The behaviour of the longitudinal phase plane is different from the one seen in the previous figure, and it can be modified by tuning the sextupole configuration.

With this configuration particles within ± 1% of energy deviation and within $3\sigma_x$ are inside 1 mm of path length difference and those within $3\sigma_y$ inside 2 mm.

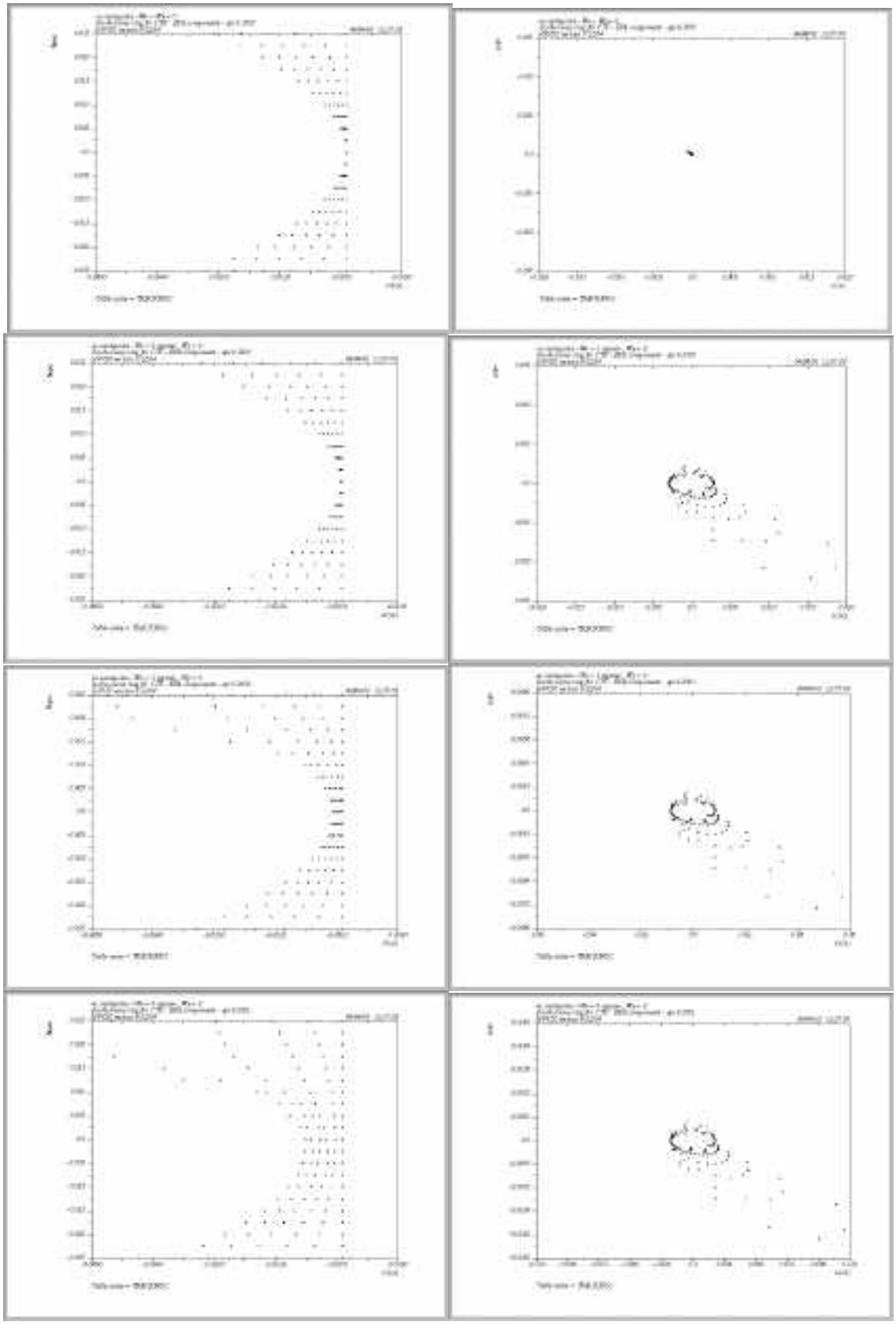

Figure 11: Path length with energy deviation and horizontal phase plane with sextupoles off.

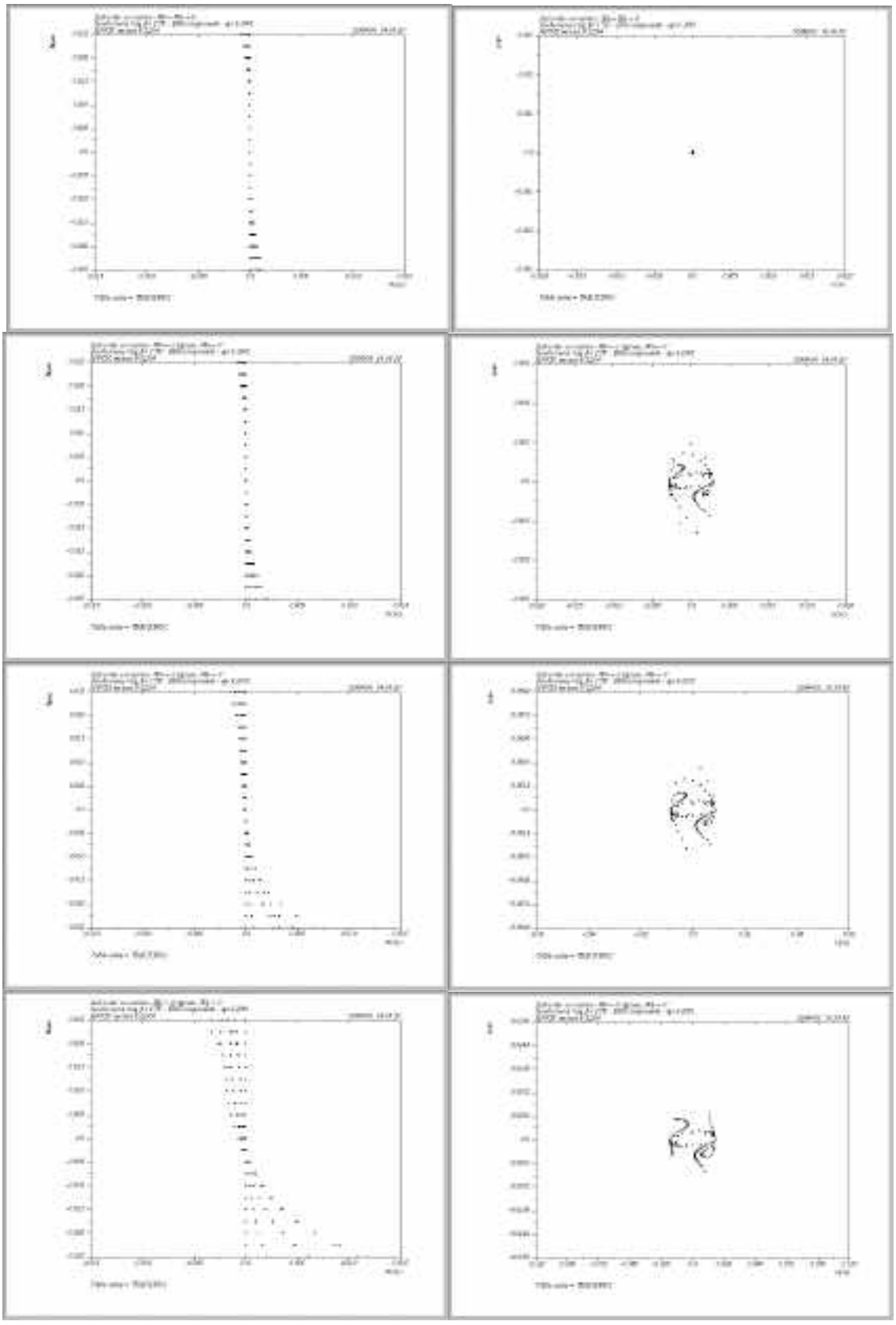

Figure 12: Path length with energy deviation and horizontal phase plane with sextupoles on.

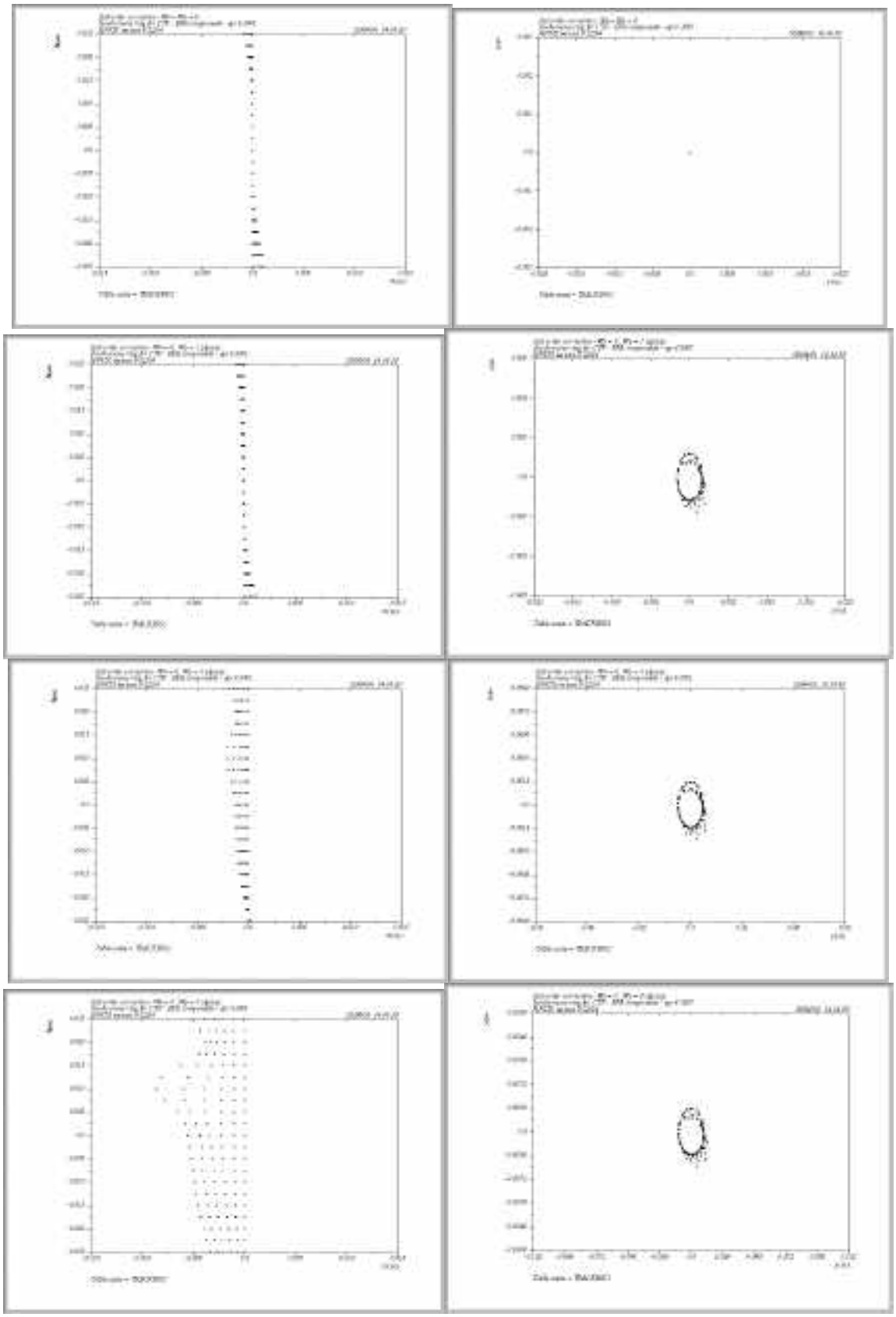

Figure 13: Path length with energy deviation and vertical phase plane with sextupoles on.

References

[1] CLIC Study Team, Proposal for Future CLIC Studies and a New CLIC Test Facility (CTF3), CERN/PS 99-047 (LP) and CLIC Note 402 (1999).

[2] F. Sannibale, CTF3 Driving Beam Delay Loop Design, CTFF3-001 Note, March 2001.

[3] C. Biscari et al, CTF3: Design of Driving Beam Combiner Ring, 7th EPAC, Vienna 26-30 June 2000.

[4] F. Sgamma, A. Beatrici, Combiner Ring layout, in preparation.

[5] LEP Preinjector Parameter List (EPA part), CERN PS/LPI Note 88-02.

[6] B. Bolli et at., Measurements on Tesla Quadrupole Prototype for the DAFNE Accumulator and Main Rings, DAFNE Technical Note MM-4, December 2, 1994.

[7] B. Bolli et at., The DAFNE Accumulator Sextupoles, DAFNE Technical Note MM-6, May 10, 1995.

[8] A. Clozza and V. Lollo, private communication.